Chinese Chemical Letters 33 (2022) 4679–4682

Contents lists available at ScienceDirect

Chinese Chemical Letters

journal homepage: www.elsevier.com/locate/cclet

Efficient ozone decomposition over bifunctional Co_3Mn-layered double hydroxide with strong electronic interaction

Bin Liu, Minxian Zhang, Jingling Yang*, Mingshan Zhu

Guangdong Key Laboratory of Environmental Pollution and Health, School of Environment, Jinan University, Guangzhou 511443, China

ARTICLE INFO

Article history:
Received 6 September 2021
Revised 8 November 2021
Accepted 11 January 2022
Available online 16 January 2022

Keywords:
Co_3Mn-layered double hydroxide
Ozone removal
Hydroxyl groups
Bifunctional catalysis
Heterogeneous catalysis

ABSTRACT

Ground-level ozone is one of the primary pollutants detrimental to human health and ecosystems. Catalytic ozone decomposition still suffers from low efficiency and unsatisfactory stability. In this work, we report a manganese-based layered double hydroxide catalyst (Co_3Mn-LDH), which exhibited a superior ozone decomposition performance with the efficiency of 100% and stability over 7 h under a GHSV of 2,000,000 mL $g^{-1}h^{-1}$ and relative humidity of 15%. Even when the relative humidity increased to 50%, the ozone decomposition also reached 86%, which significantly exceeds as-synthesized MnO_2 and commercial MnO_2 in performance. The catalytic mechanism was studied by H_2-TPR, FT-IR and XPS. The excellent performance of Co_3Mn-LDH can be attributed to its abundant surface hydroxyl groups that ensured the preferentially surface enrichment of ozone, as well as the cyclic dynamic replenishment of electrons between multivalent Co^{2+}/Co^{3+}, $Mn^{2+}/Mn^{3+}/Mn^{4+}$ and oxygen species that endowed the stable ozone decomposition. This work offers new insights into the design of efficient catalysts for ozone pollution control.

A Co_3Mn-Layered double hydroxide nanosheet was constructed to realize efficient and stable ozone decomposition through the surface enrichment of ozone by its surface hydroxyl groups and continuous ozone decomposition *via* the dynamic electron replenishment between internal Co/Mn and lattice oxygen.

Ground-level ozone (O_3) is a hazardous air pollutant that contributes to the formation of photochemical smog [1]. Due to the strong oxidizing ability of ozone, long-term exposure to atmospheric ozone can cause upper respiratory tract disease and central nervous system damage, even emphysema and pulmonary edema [2,3]. High concentrations of near-ground ozone could damage vegetation [4,5]. Moreover, the secondary organic aerosols produced by the reaction between ozone and indoor organic compound are more harmful to human health [6]. Therefore, developing a cost-effective and environment-friendly technique for reducing ozone pollution is of considerable significance and is in urgent demand.

The reported ozone removal strategies include thermal decomposition, chemical adsorption, liquid absorption and catalytic decomposition [7–9]. Among all these techniques, catalytic decomposition, as a novel, low-cost, and green technique that converts ozone to nontoxic oxygen under ambient condition, has been recognized as one of the most promising methods [10–13]. The key to the unsatisfactory performance of ozone catalytic decomposition technology lies in the following three points: (a) The low utilization of catalytic active sites on the catalyst due to the insufficient contact between O_3 and catalyst; (b) the catalyst deactivation resulting from the catalyst's valence state that changes significantly after the reaction; (c) the competitive adsorption of water on reactive sites [14,15]. Therefore, it is urgent to develop cost-effective catalysts with outstanding activities and stability.

Layered double hydroxide (LDH) as a class of clay materials, is consisted of interlayer anions and brucite-like host layers. Its metal species can be adjusted to stacks of positively charged transition metals. The highly tunable composition, facile exchangeability of intercalated anions, and uniform distribution of metal cations in the brucite-like layers endowed LDHs gain great attention in catalysis [16–21], but their exploration in air purification is rarely reported. The unique physicochemical properties of LDH, *i.e.*, abundant hydroxyl groups, variable valency, and largely exposed active sites, make it suitable for the capture of atmospheric pollutants and trigger catalytic redox reactions.

In this work, we synthesized a cobalt-manganese layered double hydroxide (Co_3Mn-LDH) as an effective ozone decomposition catalyst, of which performance is well beyond that of as-

* Corresponding author.
E-mail address: yangjl@jnu.edu.cn (J. Yang).

https://doi.org/10.1016/j.cclet.2022.01.025
1001-8417/

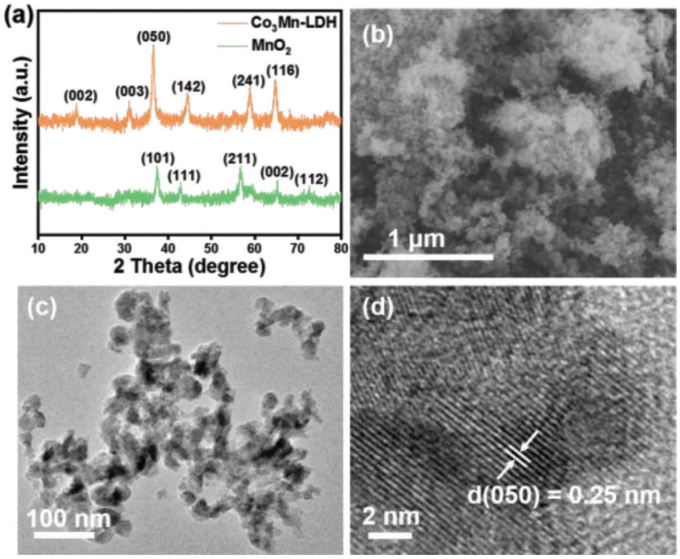

Fig. 1. (a) XRD patterns of as-prepared samples, (b) SEM image, (c) TEM image, and (d) HRTEM image of Co_3Mn-LDH.

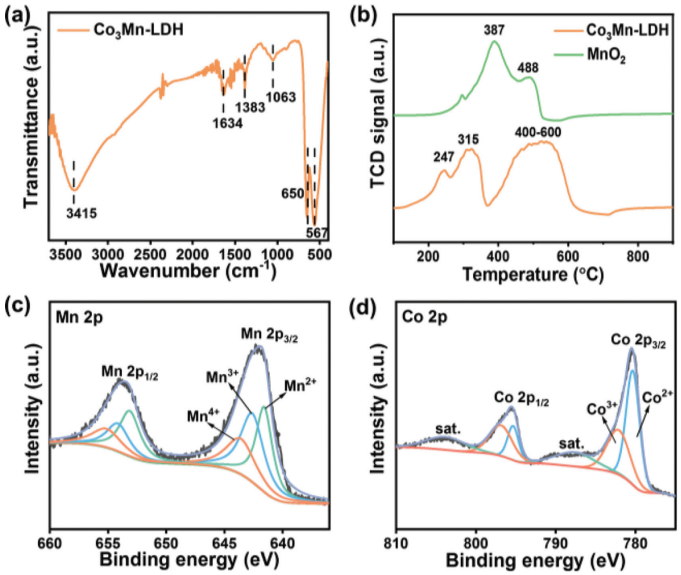

Fig. 2. (a) FT-IR spectrum, (b) H_2-TPR profiles. High-resolution XPS spectra of (c) Mn 2p and (d) Co 2p of Co_3Mn-LDH.

synthesized MnO_2 and commercial MnO_2. The performance of catalytic ozone removal by Co_3Mn-LDH under different relative humidity and the long-term catalytic stability were investigated. The relationships between the properties and catalytic activity for ozone elimination through Co_3Mn-LDH were revealed *via* H_2-TPR, FT-TR, and XPS. A mechanism for the catalytic ozone removal reaction over Co_3Mn-LDH was proposed: (a) ozone molecules were adsorbed by abundant surface hydroxyl groups on Co_3Mn-LDH; (b) the variable valencies of Co and Mn species in Co_3Mn-LDH offered abundant and well-dispersed catalytic sites for maintaining the dynamic replenishment of electrons for continuous reactions, and thus further improving the catalytic activity.

X-ray diffraction (XRD) patterns of Co_3Mn-LDH and MnO_2 are shown in Fig. 1a. The Co_3Mn-LDH planes of (002), (003), (050), (142), (241) and (116) were found at 2θ = 18.8°, 31.0°, 36.5°, 44.4°, 58.9° and 64.6°, respectively, corresponding to the typical pattern of CoMn-LDH (JCPDS No. 12-0647) [22]. MnO_2 was synthesized as a comparison, which displayed well-defined diffraction peaks corresponding to MnO_2 (JCPDS No. 50-0866). The result of X-ray diffraction (XRD) analysis revealed that the as-prepared Co_3O_4 are the pure cubic phase Co_3O_4 (JCPDS No. 42-1467) (Fig. S1 in Supporting information). Scanning electron microscopy (SEM) and transmission electron microscopy (TEM) were carried out to observe the morphology of Co_3Mn-LDH and the as-prepared MnO_2. As shown in Figs. 1b and c, the Co_3Mn-LDH is composed of nanoparticles with an average size of about 30 nm. Clearly lattice fringes can be observed in Fig. 1d. The measured lattice spacing is 0.25 nm, which matches the (050) planes of Co_3Mn-LDH. The as-synthesized MnO_2 is also composed of nanoparticles with an average particle size of *ca.* 20 nm (Fig. S2 in Supporting information).

The surface properties of Co_3Mn-LDH were further investigated by temperature-programmed reduction of hydrogen (H_2-TPR), Fourier transform infrared (FT-IR) spectrometer, and X-ray photoelectron spectroscopy (XPS). As shown in Fig. 2a, the obvious peak signal of hydroxyl groups can be observed at 3415 cm^{-1}, revealing the abundant surface hydroxyl group. It has been reported that hydroxyl group has a stronger interaction with ozone that may facilitate the surface enrichment of ozone on catalyst [23]. The peak at 1634 cm^{-1} is the bending vibration of interlayer water [24]. The small peaks at 1383 cm^{-1} and 1063 cm^{-1} correspond to the slight amount of carbonate between the layers [25]. The low-frequency peaks in the 400-800 cm^{-1} were associated with the metal-oxygen (M-O) stretch [26,27]. These results collectively confirmed that Co_3Mn-LDH had been successfully prepared.

The H_2-TPR experiments were carried out to investigate the redox ability of the samples [28], and the results are shown in Fig. 2b. The Co_3Mn-LDH sample showed two main reduction peaks. The peak in Region I (150–370 °C) can be attributed to the reduction of manganese species and the peak in Region II (400–600 °C) can be assigned to the reduction of cobalt species [29,30]. Obviously, the peaks of manganese species in Co_3Mn-LDH (247 and 315 °C) are under significantly lower temperatures compared to that of MnO_2 (387 and 488 °C), indicating the stronger reduction ability of manganese species in Co_3Mn-LDH. The broad reduction profile peak at 400–600 °C can be ascribed to the stepwise reduction of Co^{3+} to Co^{2+} and CoO to metallic cobalt [31,32]. According to the position peaks, the Co_3Mn-LDH demonstrates a strong redox ability that could be highly beneficial for catalytic ozone decomposition.

Generally, the electron distribution and chemical states of catalysts are closely related to the catalysis activity. Thus, the element states of Co_3Mn-LDH were first analyzed by XPS. The survey spectra (Fig. S3a in Supporting information) demonstrated the presence of C, O, Co, Mn in Co_3Mn-LDH. As shown in Fig. 2c, the Mn $2p_{3/2}$ peak of Co_3Mn-LDH can be deconvolved into three peaks with the binding energy at 641.6, 642.6 and 643.6 eV, corresponding to Mn(II), Mn(III) and Mn(IV) [33,34] with proportions of 34.8%, 39.1%, 26.1%, respectively. Moreover, the corresponding ratio of (Mn(II) + Mn(III))/Mn(IV) in Co_3Mn-LDH is 2.83:1, much higher than that of MnO_2 (ratio = 2.21:1, Fig. S4 and Table S1 in Supporting information). The abundant Mn(II) and Mn(III) species coexisted in Co_3Mn-LDH, which could favor the redox reactions [10]. As for the Co 2p spectra (Fig. 2d), the binding energies of Co $2p_{3/2}$ at 780.4 and 782.1 eV and the Co $2p_{1/2}$ at 795.3 and 797.0 eV indicate the presence of Co^{2+} and Co^{3+} in several. The relative peak intensity of Co^{2+}/Co^{3+} was calculated to be 60.3/39.7. Beyond that, the peaks at both 787.9 and 804.1 eV were denoted to the satellite peaks [35]. A great number of low-valence Mn and Co species

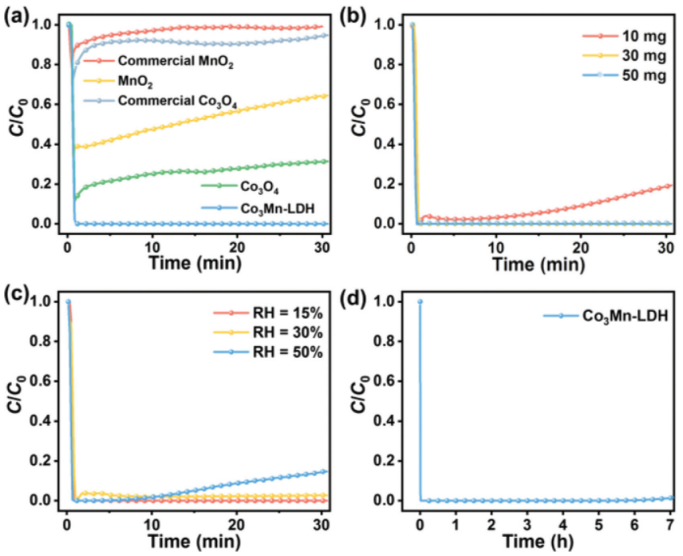

Fig. 3. The catalytic performance of the samples. (a) The ozone removal rate of Co_3Mn-LDH, as-prepared MnO_2, as-prepared Co_3O_4, commercial MnO_2 and commercial Co_3O_4. (b) The ozone removal rate of Co_3Mn-LDH with different dosages. (c) The ozone removal rate of Co_3Mn-LDH under different relative humidity conditions. (d) Long-term experiment of ozone removal by Co_3Mn-LDH. (Ozone initial concentration of 60 ppm, temperature = 25 °C, GHSV of 2000,000 mL $g^{-1}h^{-1}$, RH = 15%).

exist in Co_3Mn-LDH, which may play a vital role in the ozone decomposition reaction. As for the O 1s spectra (Fig. S3b in Supporting information), the binding energies at 530.1, 531.5 and 532.3 eV can be ascribed to the lattice oxygen (O_{Latt}), the surface adsorbed oxygen (O_{ads}) and the hydroxyl/carbonate oxygen, respectively [36–38].

The O_3 decomposition performance of Co_3Mn-LDH was evaluated under the ambient conditions with a relative humidity (RH) of 15%, inlet O_3 concentration of 60 ppm, and gas hourly space velocity (GHSV) of 2000,000 mL g^{-1} h^{-1} (Fig. S5 in Supporting information). Notably, the ozone decomposition efficiency of Co_3Mn-LDH reached 100% in 30 min (Fig. 3a). The commercial Co_3O_4 is insufficient to decompose ozone (removal rate of 8%), and the ozone removal efficiency of as-prepared Co_3O_4 (69%) is obviously lower than that of Co_3Mn-LDH (100%). Furthermore, the commercial MnO_2 could not effectively decompose ozone (removal rate of 2%), while for MnO_2, the efficiency of ozone removal decreased from 61% to 36% in 30 min. The ozone removal rate of Co_3Mn-LDH is almost 3-folds that of the as-prepared MnO_2, and far exceeds that of the commercial MnO_2. The catalytic performance comparison of Co_3Mn-LDH with that of previously reported catalysts in Table S2 (Supporting information), the present Co_3Mn-LDH catalyst achieved a 100% removal rate under a high GHSV of 2000,000 mL h^{-1} g^{-1}, while most reported studies are limited to a lower GHSV or conversion of ozone.

The effect of catalyst dosage on ozone removal efficiency was investigated. As the dosage of catalyst increased from 10 mg to 50 mg, the removal efficiency of ozone within 30 min increased from 81% to 100% (Fig. 3b). The excessive supply of catalyst to dosage above 30 mg resulted in poor utilization of reactive sites and high cost. Therefore, 30 mg was chosen as the optimum catalyst dosage.

Water vapor has a passive impact on catalytic performance in ozone decomposition, which could adsorb on the active site and hinder the adsorption of ozone molecules [39]. Here, we investigated the ozone conversion performance on Co_3Mn-LDH under different relative humidity (RH) conditions (RH = 15%−70%). As RH increased from 15% to 30%, the ozone removal efficiency remained stable at nearly 100% (Fig. 3c). As the RH continued to rise to 70%, the ozone removal efficiency gradually decreased from 86% under RH = 50% to 63% under RH = 70% (Fig. S6 in Supporting information), which might be caused by the competitive adsorption of H_2O molecule on catalyst that led to an inhibition of the ozone uptake [11,40]. The results revealed that the Co_3Mn-LDH catalyst is resistible to moisture condition (RH = 15%−50%).

Stability can be a critical assessment index in practical application. Here, the long-term photocatalytic stability test for Co_3Mn-LDH was carried out. As shown in Fig. 3d, the ozone removal efficiency of Co_3Mn-LDH remained stable at 100% after running for 7 h. We have checked the morphology and structure of the Co_3Mn-LDH catalyst after reaction by TEM microscopy and XRD. The morphology of the used catalyst is almost unchanged compared with the fresh sample (Fig. S8 in Supporting information). The XRD pattern (Fig. S9 in Supporting information) shows that there were no significant differences between the fresh and the used Co_3Mn-LDH catalyst, indicating the outstanding structure stability of Co_3Mn-LDH [41]. We have conducted the FT-IR to investigate the change of the surface property of the Co_3Mn-LDH before and after the reaction. As shown in Fig. S10 (Supporting information), we found that the peak (3415 cm^{-1}) became slightly weaker after the reaction, which may be attributed to a small amount of surface hydroxyl groups (−OH) group consumed by the reaction. However, the peak corresponds to peroxide species (1380 cm^{-1}) increased after reaction [39], which indicates the introduced O_3 can be decomposed to peroxide species over Co_3Mn-LDH that involved in the catalytic process. Moreover, the XPS spectra of Co_3Mn-LDH after reaction (Fig. S7 and Table S1 in Supporting information) reveal the negligible variation of the valence state. The electrostatic redox couple between Mn/Co may play a key role in ensuring the sustainability of catalytic ozone removal, which is discussed in detail below.

According to the changes of the chemical surface state of the used Co_3Mn-LDH (Fig. S7 and Table S1) and the mechanism of catalytic ozone removal we reported in previous works [10,11,33], the ozone decomposition mechanism of Co_3Mn-LDH is proposed: During reactions, the relative molar ratio of (Mn(II) + Mn(III))/Mn(IV) decreased from 2.83 to 2.76, with Co(II)/Co(III) ratio slightly declining from 1.55 to 1.52, suggesting both Mn(II)/Mn(III) and Co(II) were the primary suppliers of electrons to activate ozone (Fig. S7 and Table S1). Nevertheless, the (Mn(II) + Mn(III))/Mn(IV) ratio of the contrast sample MnO_2 sharply decreased from 2.22 to 1.24 after reaction.

Therefore, the relatively stable molar ratio of (Mn(II) + Mn(III))/Mn(IV) in Co_3Mn-LDH during the reaction stage suggested that a spontaneous electron transfer from the low valence Co(II) to Mn species in Co_3Mn-LDH induced the relative stable valence sate of (Mn(II) + Mn(III))/Mn(IV). The ratio of $O_{Latt}/(O_{ads} + O_{surf})$ reduced from 2.79 to 2.50 after reaction, which can be explained by the oxidation of O_{Latt} to O_{ads} with the reduction of the oxidized Mn(IV)/Co(III) to Mn(II) + Mn(III)/Co(II) to complete the redox reaction and maintain the electrostatic balance.

Consequently, the mechanisms for the catalytic process over Co_3Mn-LDH were proposed in Fig. 4. As a dipole molecule, ozone has both nucleophilic site and electrophilic site [23,42]. Ozone molecules may combine with the H (electrophilic) and O (nucleophilic) atoms of the surface hydroxyl group on Co_3Mn-LDH during their interaction [33,43]. First, the ozone molecules were fixed on the −OH group of Co_3Mn-LDH. Then, the transformation of Mn(II)/Mn(III) to Mn(IV) and Co(II) to Co(III) supplied the electrons for sustainable catalytic ozonation (Eqs. 1–4), and the consumed electrons were replenished *via* the charge-transfer of Co(II) → Co(III) (Eq. 5) and $O_{Latt} \rightarrow O_2$, maintaining the electrostatic balance in Co_3Mn-LDH (Eq. 6).

$$\mathrm{Mn(II)/Mn(III)} + O_3 \rightarrow \mathrm{Mn(IV)} + \left[O^{2-}\right]_{ads} + O_2 \quad (1)$$

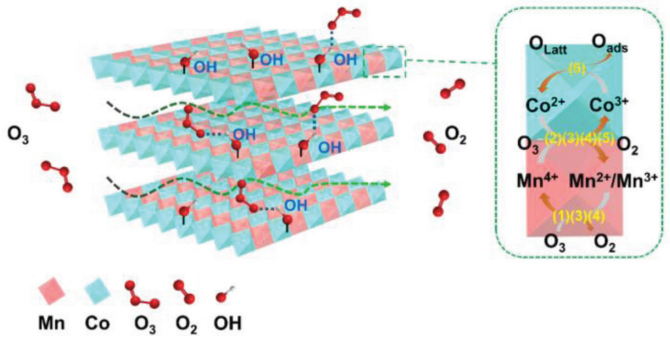

Fig. 4. The plausible mechanism of ozone decomposition over Co_3Mn-LDH.

$$Co(II) + O_3 \rightarrow Co(III) + \left[O^{2-}\right]_{ads} + O_2 \quad (2)$$

$$O_3 + \left[O^{2-}\right]_{ads} \rightarrow O_2 + \left[{O_2}^{2-}\right]_{ads} \quad (3)$$

$$\left[{O_2}^{2-}\right]_{ads}{}^{*} \rightarrow O_2 + * \quad (4)$$

$$Mn(IV) + Co(II) \rightarrow Mn(II)/Mn(III) + Co(III) \quad (5)$$

$$Mn(IV) + Co(III) + O_{Latt} \rightarrow Mn(II)/Mn(III) + Co(II) + O_{ads} \quad (6)$$

In this study, we have demonstrated a novel Co_3Mn-LDH material for efficient ozone decomposition. Under a GHSV of 2000,000 mL g^{-1} h^{-1}, the Co_3Mn-LDH catalyst displayed a stable ozone decomposition efficiency of 100% and excellent stability over 7 h, which is almost 3-folds enhanced catalytic activity of MnO_2. Even if the relative humidity increased to 50%, the ozone decomposition also reached 86%. Based on the results of the above-mentioned analysis, the excellent ozone catalytic performance of Co_3Mn-LDH are supposed to be mainly ascribed to the following cooperative effects: (a) The abundant hydroxyl groups on the surface facilitated the surface enrichment of ozone molecules, thereby promoting the effective decomposition of ozone on Co_3Mn-LDH; (b) The multivalence states of Co/Mn of Co_3Mn-LDH offered abundant and well-dispersed catalytic sites for maintaining the dynamic replenishment of electrons for continuous reactions, thus further improving the catalytic activity. The findings offer us a new perspective for the development of low-cost, easy-to-process, and highly efficient clay material as an ozone decomposition catalyst for practical application.

Declaration of competing interest

The authors declare that they have no known competing financial interests or personal relationships that could have appeared to influence the work reported in this paper.

Acknowledgments

The study was financially supported by the National Natural Science Foundation of China (No. 21320064) and the Science and Technology Program of Guangzhou (No. 202102020325).

Supplementary materials

Supplementary material associated with this article can be found, in the online version, at doi:10.1016/j.cclet.2022.01.025.

References

[1] O.R. Cooper, D.D. Parrish, A. Stohl, et al., Nature 463 (2010) 344–348.
[2] C.S. Kim, N.E. Alexis, A.G. Rappold, et al., Am. J. Resp. Crit. Care 183 (2011) 1215–1221.
[3] H. Liu, S. Liu, B. Xue, et al., Atmos. Environ. 173 (2018) 223–230.
[4] Z. Feng, E. Hu, X. Wang, L. Jiang, X. Liu, Environ. Pollut. 199 (2015) 42–48.
[5] A.S. Lefohn, C.S. Malley, H. Simon, et al., Atmos. Environ. 152 (2017) 123–145.
[6] P. Wolkoff, C.K. Wilkins, P.A. Clausen, G.D. Nielsen, Indoor Air 16 (2006) 7–19.
[7] L. Zhou, C. Richard, C. Ferronato, J.M. Chovelon, M. Sleiman, Chem. Eng. J. 334 (2018) 2098–2104.
[8] S.W. Benson, A.E. Axworthy, J. Chem. Phys. 26 (1957) 1718–1726.
[9] M. Namdari, C.S. Lee, F. Haghighat, Build. Environ. 187 (2021) 107370.
[10] Z. Lian, J. Ma, H. He, Catal. Commun. 59 (2015) 156–160.
[11] G. Zhu, J. Zhu, W. Jiang, et al., Appl. Catal. B: Environ. 209 (2017) 729–737.
[12] X. Li, J. Ma, H. He, J. Environ. Sci. 94 (2020) 14–31.
[13] A. Naydenov, P. Konova, P. Nikolov, et al., Catal. Today 137 (2008) 471–474.
[14] C. Jiang, P. Zhang, B. Zhang, J. Li, M. Wang, Ozone-Sci. Eng. 35 (2013) 308–315.
[15] Z.B. Sun, Y.N. Si, S.N. Zhao, Q.Y. Wang, S.Q. Zang, J. Am. Chem. Soc. 143 (2021) 5150–5157.
[16] W. Ye, X. Fang, X. Chen, D. Yan, Nanoscale 10 (2018) 19484–19491.
[17] S. Kosasang, N. Ma, P. Wuamprakhon, et al., Chem. Commun. 54 (2018) 8575–8578.
[18] N. Ma, S. Kosasang, A. Krittayavathananon, et al., Chem. Commun. 55 (2019) 1213–1216.
[19] Y. Yang, Y. Ou, Y. Yang, et al., Nanoscale 11 (2019) 23296–23303.
[20] X. Guo, Z. Fan, Y. Wang, Z. Jin, Surf. Interfaces 24 (2021) 101105.
[21] F.Z. Janani, N. Taoufik, H. Khiar, et al., Surf. Interfaces 25 (2021) 101263.
[22] Y. Guo, S. Zhang, J. Wang, Z. Liu, Y. Liu, J. Alloys Compd. 832 (2020) 154899.
[23] F. Qi, Z. Chen, B. Xu, et al., Appl. Catal. B: Environ. 84 (2008) 684–690.
[24] M. Li, L. Li, S. Lin, Chin. Chem. Lett. 31 (2020) 1511–1515.
[25] S. He, R. Yin, T. Lai, et al., Chemosphere 266 (2021) 129006.
[26] J. Zhao, J. Chen, S. Xu, et al., J. Mater. Chem. A 1 (2013) 8836–8843.
[27] S. He, R. Yin, Y. Chen, et al., Chem. Eng. J. 423 (2021) 130172.
[28] J. Xiong, Z. Li, P. Zhang, et al., Chin. Chem. Lett. 32 (2021) 1447–1450.
[29] S. Liang, F. Teng, G. Bulgan, R. Zong, Y. Zhu, J. Phys. Chem. C 112 (2008) 5307–5315.
[30] C. Shi, Y. Wang, A. Zhu, B. Chen, C. Au, Catal. Commun. 28 (2012) 18–22.
[31] L. Huang, X. Hu, S. Yuan, et al., Appl. Catal. B: Environ. 203 (2017) 778–788.
[32] Z. Zhu, G. Lu, Z. Zhang, et al., ACS Catal. 3 (2013) 1154–1164.
[33] J. Yang, Y. Huang, Y.W. Chen, et al., Nano Today 35 (2020) 100944.
[34] X. Hu, L. Huang, J. Zhang, et al., J. Mater. Chem. A 6 (2018) 2952–2963.
[35] L. Zhang, C. Yang, Z. Xie, X. Wang, Appl. Catal. B: Environ. 224 (2018) 886–894.
[36] G. Zhu, J. Zhu, W. Li, et al., Environ. Sci. Technol. 52 (2018) 8684–8692.
[37] S. Mo, P. Peng, Y. Pei, et al., Chin. Chem. Lett. 32 (2021) 2057–2060.
[38] S. Wang, Y. Zhu, Y. Zhang, et al., Nanoscale 12 (2020) 12817–12823.
[39] G. Zhu, W. Zhu, Y. Lou, et al., Nat. Commun. 12 (2021) 4152.
[40] C. Wang, J. Ma, F. Liu, H. He, R. Zhang, J. Phys. Chem. C 119 (2015) 23119–23126.
[41] S. Nimai, H. Zhang, Z. Wu, N. Li, B. Lai, Chin. Chem. Lett. 31 (2020) 2657–2660.
[42] M. Tian, S. Liu, L. Wang, et al., Environ. Sci. Technol. 54 (2020) 1938–1945.
[43] T. Zhang, C. Li, J. Ma, H. Tian, Z. Qiang, Appl. Catal. B: Environ. 82 (2008) 131–137.